Three-dimensional nanoporous copper with tunable structure prepared by dealloying titanium–copper–cobalt metallic glasses for supercapacitors

Xiang Yue[1], Rui Hu[2], Jiqiu Qi[1] ✉, Yanwei Sui[1], Yezeng He[1], Qingkun Meng[1], Fuxiang Wei[1], Yaojian Ren[1], Yulong Zhao[1]

[1]*School of Materials Science and Engineering, China University of Mining and Technology, Xuzhou 221116, People's Republic of China*
[2]*State Key Laboratory of Solidification Processing, Northwestern Polytechnical University, Xian 710072, People's Republic of China*
✉ *E-mail: flower_cumt@outlook.com*

Published in Micro & Nano Letters; Received on 16th October 2019; Revised on 6th December 2019; Accepted on 15th January 2020

Three-dimensional bicontinuous nanoporous copper (NPC) with a pore size of 10–60 nm was fabricated by dealloying titanium–copper–cobalt amorphous ribbons in 0.23 M hydrofluoric acid (HF) solution for 1–12 h. It is found that dealloyed ribbons show sandwich-like layered structure in the cross-section and the pore size in the outer layer is larger than that in the core layer. The NPC ribbons, polarised in 1 M potassium hydroxide (KOH) solution for 30 min, delivered an excellent electrochemical performance with a specific capacitance of 202.3 mF/cm^2 at the current density of 5 mA/cm^2 in 1 M KOH electrolyte and good cycling stability of 90% capacitance retention after 5000 cycles at 20 mA/cm^2.

1. Introduction: As an electrochemical energy storage device, the supercapacitor has many advantages such as high-energy density and fast charge and discharge [1–3]. The electrode material plays a decisive role in the entire supercapacitor device [4, 5]. In recent years, some scholars have developed the metal corrosion oxidation route to prepare nanoporous electrode materials, which directly grow on the metal substrates [6]. Three-dimensional (3D) bicontinuous nanoporous structures can be obtained by dealloying crystalline metals, and pore and ligament size can be controlled by changing alloy composition, solution concentration, temperature and corrosion time. Meanwhile, the ternary alloy system prepared by adding a small amount of alloying elements is receiving more attention since the third element plays an important role in the nanoporous structure [7]. As we know, little work has been performed on the preparation of nanoporous metal materials using amorphous alloys. Amorphous alloys, due to the single-phase composition, uniform structure and adjustable starting materials, can be used to prepare nanoporous materials with more uniform pore distribution compared with crystalline alloys.

The standard electrode potentials of titanium (Ti) is as much as 1972 mV higher than that of copper (Cu), indicating that Ti is easily removed in binary Ti–Cu alloys [8]. Therefore, we propose a new idea to prepare nanoporous Cu (NPC) with adjustable pore size by dealloying Ti–Cu–cobalt (Co) amorphous alloy and apply it in supercapacitor. In this work, ternary amorphous alloys with different compositions were immersed in HF solutions at different times. The composition, morphology and electrochemical properties of as-dealloyed NPC were investigated.

2. Experimental procedure: Ternary amorphous Ti–Cu–Co ingots were fabricated by arc melting pure Ti, pure Cu and Co in an argon atmosphere. The single-roller melt-spinning method was used to prepare amorphous ribbons. Chemical dealloying Ti–Cu–Co amorphous ribbons were performed in dilute HF aqueous solution with a concentration of 0.23 M at 298 K. After immersion for a given time (1, 4, 8 and 12 h), the dealloyed ribbons were taken out and well-rinsed with dehydrated alcohol and distilled water to remove the residual HF solution, respectively.

The phase composition of the as-spun Ti–Cu–Co ribbons and the NPC were investigated by X-ray diffractometer (XRD) (Bruker AXS, D8 Advance) with Cu Kα radiation. The morphology of samples was observed by a field-emission scanning electron microscope (FESEM, SU8220) equipped with energy-dispersive X-ray spectroscopy. The structures of NPC ribbons were investigated by a transmission electron microscope (TEM, Tecnai G2F20) and a high-resolution TEM (HRTEM). The analysis of the valence of the surface layers was conducted by an X-ray photoelectron spectrometer (ESCALAB 250Xi). The pore size and its distribution were analysed by Image-Pro-Plus software.

The NPC was further polarised in 1 M potassium hydroxide (KOH) solution at 0.8 V using an electrochemical workstation (CHI660E, Chenhua), in which a platinum electrode was used as counter electrode and calomel electrode as a reference electrode. After polarisation treatment, the electrochemical performance of the NPC hybrid electrode was tested in the same three-electrode system. The galvanostatic charge/discharge curves (GCD) of the electrode was measured at a current density of 5–50 mA/cm^2 and the potential window from 0 to 0.7 V.

3. Results and discussion: X-ray photoelectron spectroscopy (XPS) measurements were used to determine the chemical composition and the valence of elements of NPCs. A wide scan of the XPS spectrum of as-dealloyed $Ti_{50}Cu_{46}Co_4$ ribbons indicates the presence of carbon, oxygen (O), Ti, Cu and chlorine. No Co peaks were found in the survey spectrum (Fig. 1*c*). As shown in Fig. 1*a*, the binding energy peak at ~932 eV suggests the presence of Cu^+ or Cu^0 species because Cu 2p3/2 XPS cannot differentiate between Cu^+ and Cu^0 [9]. A low satellite peak appears between Cu 2p3/2 and 2p1/2, indicating there is a small amount of Cu–O. However, the amount of Cu_2O was relatively higher than Cu–O. In the O1s spectrum, the binding energy peaks located at 530.3 and 531.3 eV (Fig. 1*b*), corresponding to the characteristic bands of O in oxides (M–O–M) and hydroxides (OH^-), respectively. The M–O–M oxide denotes O with a Cu–O bond and OH^- represents the adsorption O on the surface of the alloy ribbons.

Fig. 1*d* shows the XRD patterns of as-spun Ti–Cu–Co ribbons and as-dealloyed $Ti_{40}Cu_{58}Co_2$ ribbons with different corrosion times. Only one single peak appearing around 41° indicated that Ti–Cu–Co alloys were in an amorphous state. Several sharp diffraction peaks can be observed for as-dealloyed $Ti_{40}Cu_{58}Co_2$ ribbons

© The Institution of Engineering and Technology 2020

with different corrosion times, which is attributed to face-centred cubic (FCC) Cu (111) (43.316°), (200) (50.448°), (220) (74.124°) (ICSD card No.: 85-1326) and Cu_2O (110) (36.574°), (200) (42.485°), (220) (61.646°) (ICSD card No.: 74-1230) [10]. The diffraction peak intensity of Cu_2O phase is different in the as-dealloyed $Ti_{40}Cu_{58}Co_2$ ribbons with different etching time. The intensity of the diffraction peak increases with the extension of corrosion time, indicating the content also increases. However, the content of Cu_2O is limited compared with Cu.

SEM morphology of as-dealloyed Ti–Cu–Co alloy ribbons in 0.23 M HF solution for different corrosion times is shown in Fig. 2. Only a few atomic layers are etched on the surface of as-dealloyed $Ti_{40}Cu_{58}Co_2$ ribbons, and a small number of regular particles belonging to Cu_2O were formed on the surface of samples. Note that corrosion first extends to irregular boundaries. 3D bicontinuous NPCs were formed in the as-dealloyed $Ti_{50}Cu_{46}Co_4$ ribbons after corrosion of 4–12 h in 0.23 M HF solution at 298 K. As shown in Figs. 2*c* and *d*, a small number of large pores with a size exceeding 100 nm can be seen, indicating that the fracture of the NPC ligament and the collapse of the pores happen as the corrosion time is further prolonged [11]. The pore size distribution (Fig. 5) also shows that the number of large pores increases with time. The pore size is mainly distributed at 4–20, 10–60, 30–120 and 10–80 nm after corrosion for 1, 4, 8 and 12 h, respectively.

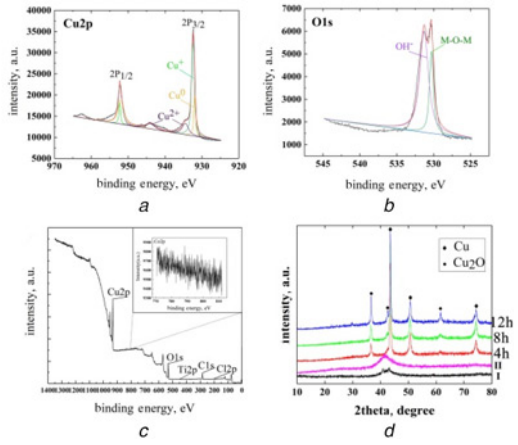


Fig. 1 *XPS survey and narrow spectra of as-dealloyed $Ti_{50}Cu_{46}Co_4$ ribbons in 0.23 M HF solution for 12 h at*
a–c 298 K
d XRD patterns of as-spun $Ti_{40}Cu_{58}Co_2$ (I) and $Ti_{50}Cu_{46}Co_4$ (II) amorphous alloys and $Ti_{40}Cu_{58}Co_2$ ribbons after dealloying in 0.23 M HF solution for 4, 8 and 12 h at 298 K

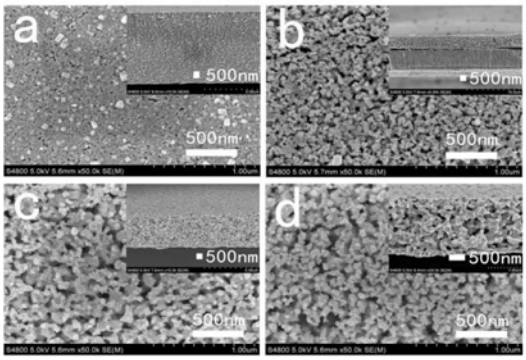


Fig. 2 *SEM morphology of as-dealloyed $Ti_{50}Cu_{46}Co_4$ ribbons after immersion of*
a 1 h in 0.23 M HF solution at 298k
b 4 h in 0.23 M HF solution at 298k
c 8 h in 0.23 M HF solution at 298k
d 12 h in 0.23 M HF solution at 298k

Compared to other literatures, the pore size of NPCs is slightly reduced by the Co addition. The nanoporosity can be regulated by the composition of starting materials and immersion time. A linear dependency of the natural logarithm of the pore size on the natural logarithm of the dealloying time is shown in Fig. 6 and the slope of the fitted lines is 0.56, close to 1/3 of the theoretical value of Cahn–Hilliard equation. This indicates that the dynamic diffusion process is related to the diffusion of interface atoms.

Dissolution of less noble Ti and recombination of noble metal Cu conducted simultaneously at the interface of the metal/electrolyte in the dealloying process. Cu atoms continually aggregate and form island or cluster structures as the corrosion time increases due to the minimisation of the surface area and curvature, which suggests the kinetics of the dissolution of Ti and Co elements in Ti–Cu–Co ternary alloy is available for the formation of NPC [12]. The hydrofluoric acid played a key role in a breakdown of the barrier of the native TiO_2 surface layer and further promoted the dissolution of internal Ti and Co elements [13]. The reaction equation is as follows [14]:

$$TiO_2 + 6F^- + 4H^+ \rightarrow [TiF_6]^{2-} + 2H_2O \quad (1)$$

$$Ti + 4HF \rightarrow TiF_4 + 2H_2 \uparrow \quad (2)$$

$$TiF_4 + 2F^- \rightarrow [TiF_6]^{2-} \quad (3)$$

As presented in insets in Fig. 2, the cross-sectional views show the NPCs immersed in 0.23 M HF solution with different times possess a 3D bicontinuous structure. The pore size increases with corrosion time, and the ligament is coarsened accordingly. The NPC ribbons ~7 μm in thickness exhibit a sandwich-like layered structure. The outer layer has a larger pore size than the core layer, which explains that the rearrangement of dissolved Cu atoms starts from the surface of NPCs. Although having similar nanoporous structures, the NPC ribbons are brittle and curly, and the sandwich-like structure is easy to fall off. The volume contraction phenomenon occurring in the dealloying process can result in the formation of cracks in ribbons specimens, which will decrease the mechanical properties and hinder the application of the nanoporous materials [15]. Methods such as low-temperature dealloying and multi-step dealloying techniques have been developed to alleviate the issue [16].

Fig. 3 shows the TEM, selected area electron diffraction pattern (SAED) and HRTEM images of as-dealloyed $Ti_{50}Cu_{46}Co_4$ ribbons

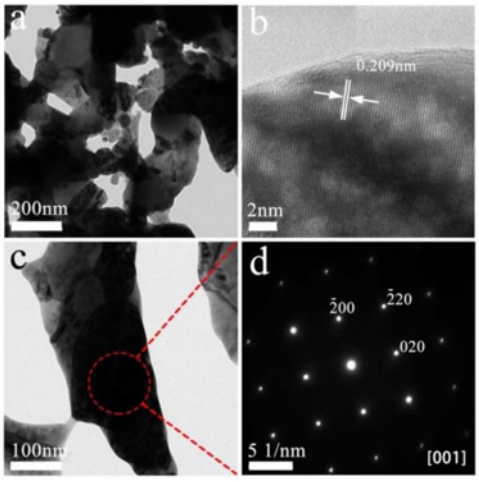


Fig. 3 *TEM*
a, c TEM images of as-dealloyed $Ti_{50}Cu_{46}Co_4$ ribbons immersed in 0.23 M HF solution for 12 h at 293 K
b HRTEM image of as-dealloyed $Ti_{50}Cu_{46}Co_4$ ribbons immersed in 0.23 M HF solution for 12 h at 293 K
d SAED pattern of as-dealloyed $Ti_{50}Cu_{46}Co_4$ ribbons immersed in 0.23 M HF solution for 12 h at 293 K

© The Institution of Engineering and Technology 2020

doi: 10.1049/mnl.2019.0627

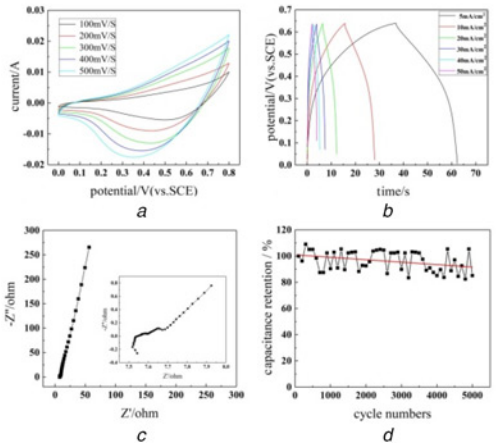


Fig. 4 *CV of the electrode at scan rates from 100 to 500 mV/s*
a CV curves of as-polarised NPC at different scanning rate
b GCD curves of as-polarised NPC at various current densities, respectively
c Typical Nyquist impedance spectrum of NPC electrodes over the frequency range of 100 kHz to 0.01 Hz and the inner is magnified
d Cycle performance of NPC-8 h electrode at a current density of 20 mA/cm^2

immersed in 0.23 M HF solution for 12 h at 293 K. The visible 3D bicontinuous porous structure was observed in Figs. 3*a* and *c*. The interplanar distance from the adjacent lattice fringes marked in Fig. 3*b* is 0.209 nm by TEM software, corresponding to the (111) planes of FCC Cu. As shown in Fig. 3*d*, the obtained NPC exhibits single-crystal feature, and the corresponding crystal ribbon axis is [001].

Fig. 4*a* illustrates the cyclic voltammogram (CV) curves of the electrode at scan rates from 100 to 500 mV/s. The similar rectangular shape of the CV curve was observed, which has small distortions in the range of scan rate. Electrical double-layer capacitor plays a major role in the electrode/electrolyte interface [17]. The area enclosed by the CV closed curve increases as the scan rate increases. Fig. 4*b* shows the GCD curves of the electrode at various current densities. The nearly linear and symmetrical curves suggest a reversible charge/discharge process. The maximum specific capacitance reaches up to 202.3 mF/cm^2 at a current density of 5 mA/cm^2. Even at a current density of 50 mA/cm^2, it can reach 148.4 mF/cm^2, which mainly attributes to the highly efficient electron/ion transfer of the nanoporous electrode [18].

The cyclic performance of as-polarised NPC electrode was evaluated by the charge/discharge testing at a current density of 20 mA/cm^2 in 1 M KOH solution, and the result is shown in Fig. 4*d*. After 5000 cycles, the specific capacitance of as-polarised NPC electrode is still more than 90% of the initial value, revealing the electrode possesses excellent long-term electrochemical stability. The electrochemical impedance spectrum consists of a semi-circle at high frequencies and a linear segment at low frequencies. As shown in Fig. 4*c*, the large slope of the straight line indicates that NPC overcomes the defect of low conductivity of ordinary active material.

4. Conclusions: Ti–Cu–Co ribbons prepared by the arc melting and single-roller melt-spinning method were dealloyed to obtain 3D bicontinuous NPCs with a pore size of 10–60 nm. As-dealloyed ribbons present a sandwich-like layered structure and the pore size and thickness of the outer layer increase with the extension of corrosion time. NPC ribbons polarised in 1 M KOH solution exhibit good electrochemical performance. The maximum areal specific capacitance reaches up to 202.3 mF/cm^2 at 5 mA/cm^2, and <10% capacitance loss is obtained after 5000 cycles at 20 mA/cm^2. Therefore, the current efforts may pave a new way to fabricate nanoporous structures for supercapacitors based on ternary amorphous alloys.

5. Acknowledgments: This work was financially supported by the National Natural Science Foundation of China (grant nos. 51601220 and 51971241) and the State Key Laboratory of Solidification Processing in NWPU (grant no. SKLSP201826).

6 References

[1] Wang R., Sui Y.W., Huang S.F., *ET AL.*: 'High-performance flexible all-solid-state asymmetric supercapacitors from nanostructured electrodes prepared by oxidation-assisted dealloying protocol', *Chem. Eng. J.*, 2018, **331**, pp. 527–535
[2] Qi J.Q., Chang Y., Sui Y.W., *ET AL.*: 'Facile synthesis of Ag-decorated Ni_3S_2 nanosheets with 3D bush structure grown on RGO and its application as positive electrode material in asymmetric supercapacitor', *Adv. Mater. Interfaces*, 2018, **5**, (3), p. 1700985
[3] Liu X., Wei F.X., Sui Y.W., *ET AL.*: 'Polyhedral ternary oxide $FeCo_2O_4$: a new electrode material for supercapacitors', *J. Alloys Compd.*, 2018, **735**, pp. 1339–1343
[4] Di J., Fu X., Zheng H., *ET AL.*: 'H–TiO_2/C/MnO_2 nanocomposite materials for high-performance supercapacitors', *J. Nanoparticle Res.*, 2015, **17**, (6), p. 255
[5] Lu X., Yu M., Wang G., *ET AL.*: 'H-TiO_2@MnO_2//H-TiO_2@C core–shell nanowires for high performance and flexible asymmetric supercapacitors', *Adv. Mater.*, 2013, **25**, (2), pp. 267–272
[6] Kang J.L., Hirata A., Qiu H.J., *ET AL.*: 'Self-grown oxyhydroxide@nanoporous metal electrode for high-performance supercapacitors', *Adv. Mater.*, 2014, **26**, (2), pp. 269–272
[7] Dan Z., Qin F., Sugawara Y., *ET AL.*: 'Nickel-stabilized nanoporous copper fabricated from ternary Ti–Cu–Ni amorphous alloys', *Mater. Lett.*, 2013, **94**, pp. 128–131
[8] Dan Z., Qin F., Sugawara Y., *ET AL.*: 'Fabrication of nanoporous copper by dealloying amorphous binary Ti–Cu alloys in hydrofluoric acid solutions', *Intermetallics*, 2012, **29**, pp. 14–20
[9] Liu P., Hensen E.J.: 'Highly efficient and robust Au/$MgCuCr_2O_4$ catalyst for gas-phase oxidation of ethanol to acetaldehyde', *J. Am. Chem. Soc.*, 2013, **135**, (38), pp. 14032–14035
[10] Dan Z., Qin F., Makino A., *ET AL.*: 'Fabrication of nanoporous copper by dealloying of amorphous Ti–Cu–Ag alloys', *J. Alloys Compd.*, 2014, **586**, pp. S134–S138
[11] Wang N., Pan Y., Wu S.K.: 'Relationship between dealloying conditions and coarsening behaviors of nanoporous copper fabricated by dealloying Cu–Ce metallic glasses', *J. Mater. Sci. Technol.*, 2018, **34**, (7), pp. 1162–1171
[12] Li Z.Q., Bai L., Lu X.: 'Inhomogeneity of bulk nanoporous silver fabricated via dealloying Ag–Zn alloy in sulphuric acid', *Micro Nano Lett.*, 2013, **8**, (11), pp. 805–808
[13] Dan Z., Qin F., Sugawara Y., *ET AL.*: 'Fabrication of nanoporous copper by dealloying amorphous binary Ti–Cu alloys in hydrofluoric acid solutions', *Intermetallics*, 2012, **29**, pp. 14–20
[14] Shrestha N.K., Schmuki P.: 'Chapter 3: electrochemistry at TiO_2 nanotubes and other semiconductor nanostructures', *Electrochemistry*, 2013, **12**, pp. 87–131
[15] Qian L.H., Chen M.W.: 'Ultrafine nanoporous gold by low-temperature dealloying and kinetics of nanopore formation', *Appl. Phys. Lett.*, 2007, **91**, (8), p. 083105
[16] Sun Y., Balk T.J.: 'A multi-step dealloying method to produce nanoporous gold with no volume change and minimal cracking', *Scr. Mater.*, 2008, **58**, (9), pp. 727–730
[17] Zheng H., Zhai T., Yu M., *ET AL.*: 'Tio_2@C core–shell nanowires for high-performance and flexible solid-state supercapacitors', *J. Mater. Chem. C*, 2013, **1**, (2), pp. 225–229
[18] Huang C., Young N.P., Grant P.S.: 'Spray processing of TiO_2 nanoparticle/ionomer coatings on carbon nanotube scaffolds for solid-state supercapacitors', *J. Mater. Chem. A*, 2014, **2**, (29), p. 11022

Appendix

On the basis of the GCD curves, the specific capacitance of as-polarised NPC electrode was calculated from the discharge curves using the following equation:

$$C_s = \frac{I \times \Delta T}{S \times \Delta V}$$

where I is the discharge current density; ΔT is the discharge time; S, ΔV and C_s represent the area, potential window and specific

© The Institution of Engineering and Technology 2020

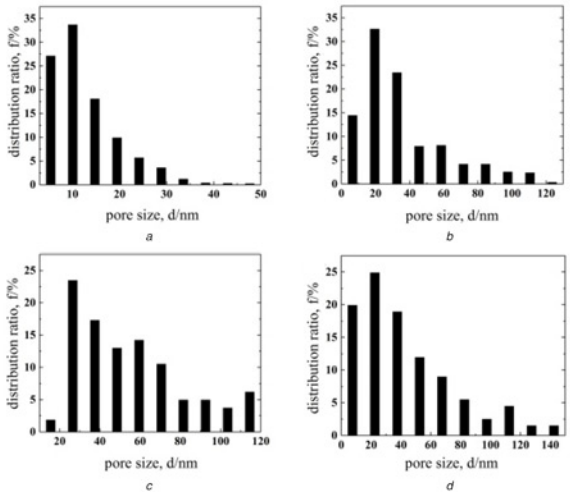


Fig. 5 *Pore size distribution of as-dealloyed $Ti_{50}Cu_{46}Co_4$ ribbons in 0.23 M HF solution for*
a 1 h at 298 K
b 4 h at 298 K
c 8 h at 298 K
d 12 h at 298 K

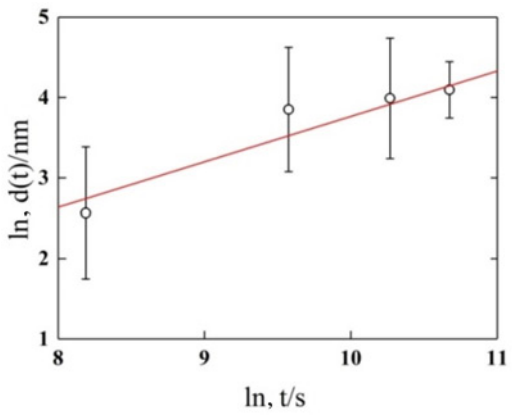


Fig. 6 *Double logarithm plot of pore size of NPC ribbons d(t) versus the dealloying time t in 0.23 M HF solution at 298 K*

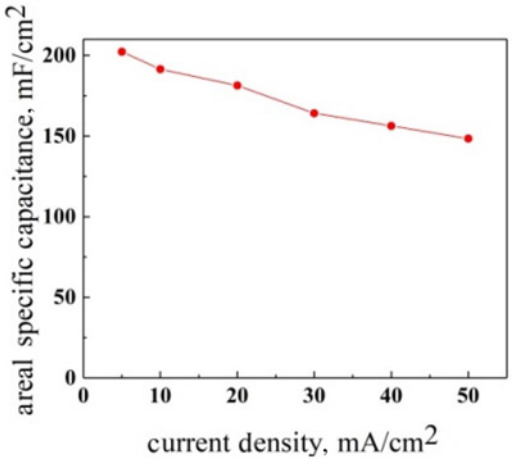


Fig. 7 *Areal specific capacitance of as-polarised NPC electrode versus current density*

Table 1 Determination results of leachates

Element	Obtained concentration value, µg/l	relative standard deviation (RSD), %
Ti	342,284	0.59
Co	24,517	3.40
Cu	2397	4.09

capacitance of electrodes, respectively. The specific capacitances are calculated to be 202.3, 191.4, 181.3, 164.1, 156.3 and 148.4 mF/cm^2 at current densities of 5, 10, 20, 30, 40 and 50 mA/cm^2, respectively (Fig. 7).

The concentrations of the Ti, Cu and Co in the leachates from the HF treatments are shown in Table 1. It can be seen that the concentrations of Ti, Cu and Co in the filtrate after HF treatment are 342284, 24517 and 2397 µg/l, respectively. Ti and Co concentrations are one and two orders of magnitudes higher than the concentration of Cu, respectively, indicating that it is feasible to dealloy Ti and Co elements in HF solution in ternary Ti–Cu–Co alloys.

© The Institution of Engineering and Technology 2020

doi: 10.1049/mnl.2019.0627